magnetoresistive component in CMR materials arising at grain boundaries at high temperatures.

Our highly symmetric Wheatstone-bridge structures afford new insight into the underlying mechanisms that contribute to CMR phenomena. The technique is able to isolate the specific contribution of a single grain boundary and quantify the role of the imposed magnetic substructure. In addition, the discovery of a positive magnetoresistance at higher temperatures underlines the significance of the cross-over between transport regimes near T_c. The dramatic effect induced by the introduction of a single grain boundary demonstrates the extreme sensitivity of the electrical conduction processes in CMR materials to microstructural defects, and the results should stimulate further experimental and theoretical study of these materials.

The potential applications of CMR materials have been limited up to now by the very high magnetic fields required to induce significant changes in resistance. Our findings immediately provide a method by which controllable low-field magnetoresistive devices may be simply fabricated from CMR materials. Moreover, such devices would have the potential to operate beyond the narrow range of operating temperatures of more simply configured CMR material systems and at lower absolute resistivities. The fields required to induce the low-field magnetoresistance in the grain boundary devices are comparable to those required for existing magnetoresistive structures such as spin valves. The use of high-T_c materials (such as $La_{0.7}Sr_{0.3}MnO_3$) should permit room-temperature operation, and a greater understanding of the basic physics and improvements in materials properties are likely to increase the magnetoresistance achievable. □

Received 4 February; accepted 25 March 1997.

1. Jin, S. *et al.* Thousandfold change in resistivity in magnetoresistive La–Ca–Mn–O films. *Science* **264,** 413–415 (1994).
2. von Helmholt, R., Wecker, J., Holszapfel, B., Schultz, L. & Samwer, K. Giant negative magnetoresistance in perovskitelike $La_{2/3}Ba_{1/3}MnO_x$ ferrmomagnetic films. *Phys. Rev. Lett.* **71,** 2331–2334 (1993).
3. Subramanian, M. A. *et al.* Colossal magnetoresistance without Mn^{3+}/Mn^{4+} double exchange in the stoichiometric pyrochlore $Tl_2Mn_2O_7$. *Science* **273,** 81–84 (1996).
4. Ramirez, A. P., Cava, R. J. & Krajewski, J. Colossal magnetoresistance in Cr-based chalcogenide spinels. *Nature* **386,** 156–159 (1997).
5. Jonker, G. H. & van Santen, J. H. Ferromagnetic compounds of manganese with perovskite structure. *Physica* **16,** 337–349 (1950).
6. Zener, C. Interaction between the *d*-shells in the transition metals. II. Ferromagnetic compounds of manganese with perovskite structure. *Phys. Rev.* **82,** 403–405 (1951).
7. Anderson, P. W. & Hasegawa, H. Considerations on double exchange. *Phys. Rev.* **100,** 675–681 (1955).
8. de Gennes, P.-G. Effects of double exchange in magnetic crystals. *Phys. Rev. B.* **118,** 141–154 (1960).
9. Furukawa, N. Transport properties of the Kondo lattice model in the limit $S = \infty$ and $D = \infty$. *J. Phys. Soc. Jpn* **63,** 3214–3217 (1994).
10. Hwang, H. Y., Cheong, S.-W., Radaelli, P. G., Marezio, M. & Batlogg, B. Lattice effects on the magnetoresistance in doped $LaMnO_3$. *Phys. Rev. Lett.* **75,** 914–917 (1995).
11. Hundley, M. F. *et al.* Transport-magnetism correlations in the ferromagnetic oxide $La_{0.7}Ca_{0.3}MnO_3$. *Appl. Phys. Lett.* **67,** 860–862 (1995).
12. Hwang, H. Y., Cheong, S.-W., Ong, N. P. & Batlogg, B. Spin-polarised intergrain tunnelling in $La_{2/3}Sr_{1/3}MnO_3$. *Phys. Rev. Lett.* **77,** 2041–2044 (1996).
13. Gupta, A. *et al.* Grain-boundary effects on the magnetoresistance properties of perovskite manganite films. *Phys. Rev. B* **54,** R15629–R15632 (1996).
14. Snyder, G. J., Hiskes, R., DiCarolis, S., Beasley, M. R. & Geballe, T. H. Intrinsic electrical transport and magnetic properties of $La_{0.67}Ca_{0.33}MnO_3$ and $La_{0.67}Sr_{0.33}MnO_3$ MOCVD thin films and bulk material. *Phys. Rev. B* **53,** 14434–14444 (1996).
15. Lu, Y. *et al.* Large magnetotunnelling effect at low magnetic fields in micrometer-scale epitaxial $La_{0.67}Sr_{0.33}MnO_3$ tunnel junctions. *Phys. Rev. B* **54,** R8357–R8360 (1996).
16. Sun, J. Z. *et al.* Observation of large low-field magnetoresistance in trilayer perpendicular transport devices made using doped manganite perovskites. *Appl. Phys. Lett.* **69,** 3266–3268 (1996).
17. Dimos, D., Chaudhari, P. & Mannhart, J. Superconducting transport-properties of grain-boundaries in $YBa_2Cu_3O_7$ bicrystals. *Phys. Rev. B* **41,** 4038–4049 (1990).
18. Beck, A. *et al.* Fabrication and superconducting transport properties of bicrystal grain boundary Josephson junctions on different substrates. *IEEE Trans. Appl. Supercond.* **5,** 2192–2195 (1995).
19. McCormack, M. *et al.* Very large magnetoresistance in perovskite-like La–Ca–Mn–O thin films. *Appl. Phys. Lett.* **64,** 3045–3047 (1994).
20. Sun, J. Z., Krusin-Elbaum, L., Parkin, S. S. P. & Xiao, G. Transport and magnetic properties of *in situ* grown thin-film La–Y–Ca–Mn–O. *Appl. Phys. Lett.* **67,** 2726–2728 (1995).
21. Xiong, G. *et al.* Giant magnetoresistance in epitaxial $Nd_{0.7}Sr_{0.3}MnO_{3-\delta}$ thin films. *Appl. Phys. Lett.* **66,** 1427–1429 (1995).
22. Parkin, S. S. P., Bhadra, R. & Roche, K. P. Oscillatory magnetic exchange coupling through thin copper layers. *Phys. Rev. Lett.* **66,** 2152–2155 (1991).
23. Dieny, B. Classical-theory of giant magnetoresistance in spin-valve mutlilayers—influence of thicknesses, number of periods, bulk and interfacial spin-dependent scattering. *J. Phys. Condens. Matt.* **4,** 8009–8020 (1992).

Acknowledgements. We thank Z. H. Barber, W. E. Booij, M. J. Hall, S. Kovtonyuk, D. B. Jardine, D.-J. Kang, E. J. Tarte, Y. S. Soman and R. E. Somekh. This work was supported by the UK EPSRC through the Advanced Magnetics Programme.

Correspondence and requests for materials should be addressed to N.D.M. (e-mail: ndm12@cus.cam.ac.uk).

Synthesis of epothilones A and B in solid and solution phase

K. C. Nicolaou*, N. Winssinger*, J. Pastor*, S. Ninkovic*, F. Sarabia*, Y. He*, D. Vourloumis*, Z. Yang*, T. Li, P. Giannakakou† & E. Hamel‡

* *Department of Chemsitry and The Skaggs Institute for Chemical Biology, The Scripps Research Institute, 10550 North Torrey Pines Road, La Jolla, California 92037, USA, and Department of Chemistry and Biochemistry, University of California San Diego, 9500 Gilman Drive, La Jolla, California 92093, USA*

† *Medicine Branch, DCS, NCI, National Institutes of Health, Bethesda, Maryland 20892, USA*

‡ *Laboratory of Drug Discovery Research and Development, Developmental Therapeutics Program, DCTDC, NCI, Frederick Cancer Research and Development Center, Frederick, Maryland 21702, USA*

Epothilones A and B, two compounds that have been recently isolated[1] from myxobacterium *Sorangium cellulosum* strain 90, have generated intense interest[2–16] among chemists, biologists and clinicians owing to the structural complexity, unusual mechanism of interaction with microtubules and anticancer potential of these molecules. Like taxol* (refs 17, 18), they exhibit cytotoxicity against tumour cells by inducing microtubule assembly and stabilization[3,4], even in taxol-resistant cell lines. Following the structural elucidation of these molecules by X-ray crystallography in 1996[1], several syntheses of epothilones A (refs 12–16) and B (ref. 19) have been reported, indicative of the potential importance of these molecules in the cancer field. Here we report the first solid-phase synthesis of epothilone A, the total synthesis of epothilone B, and the generation of a small epothilone library. The solid-phase synthesis applied here to epothilone A could open up new possibilities in natural-product synthesis and, together with solution-phase synthesis of other epothilones, paves the way for the generation of large combinatorial libraries of these important molecules for biological screening.

The strategy for the solid-phase synthesis of epothilone A (**1**) was based on the retrosynthetic analysis indicated in Fig. 1 (refs 5, 13). Thus, it was anticipated that the three requisite fragments (**5**–**7**), one on a solid support (**7**), would be coupled together sequentially through an aldol reaction, an esterification reaction, and an olefin metathesis reaction[20–25], the latter simultaneously cyclizing and liberating the product from the solid support (**6** + **7** + **5** → **4** → **3**). A simple desilylation and epoxidation reaction would then complete the total synthesis of epothilone A (**1**) and analogues thereof (**3** → **1**). The outlook for obtaining two products at each of the aldol, metathesis and epoxidation steps was considered advantageous for the purposes of library generation.

Merrifield resin (**8**, Fig. 2) was converted to phosphonium salt **9** in >90% yield by sequential reaction with: (1) 1,4-butanediol-NaH-*n*-Bu_4NI cat.: (2) Ph_3P-iodine-imidazole; and (3) Ph_3P (for abbreviations see figure legends). Ylide **10**[26], generated from **9** by the action of NaHMDS in THF : DMSO at 25 °C, reacted with aldehyde **11** (K.C.N. *et al.*, unpublished results) at 0 °C to form olefinic compound **12** in >70% yield. The geometry of the double bond in **12** was tentatively[14] assigned as *Z*, but its geometry was neither rigorously determined nor did it matter for our purposes. Desilylation of **12** with HF·pyridine, followed by Swern oxidation of the resulting primary alcohol furnished aldehyde **7** in high yield (>95%). The aldol condensation of the polymer-bound aldehyde **7** with the dianion derived from keto acid **6** in the presence of $ZnCl_2$ in tetrahydrofuran (THF) gave a mixture of diastereoisomers

* Bristol-Myers Squibb has registered Taxol as a trademark and wishes the sceintific community to use the name paclitaxel.

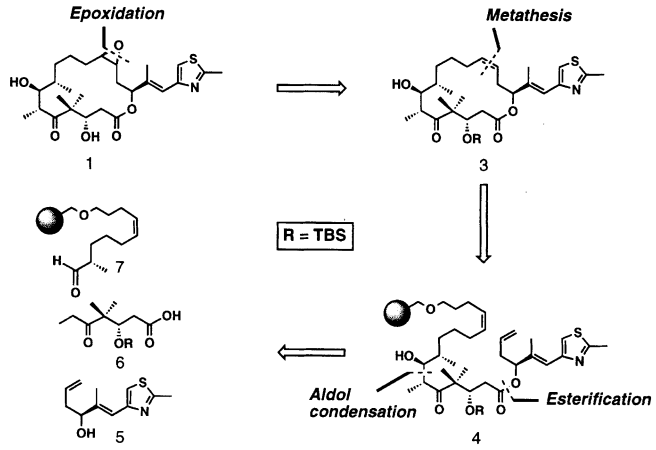

Figure 1 Retrosynthetic analysis of epothilone A (**1**) by a solid-phase olefin metathesis strategy. TBS, *t*-$BuMe_2Si$; the shaded circle indicates polystyrene.

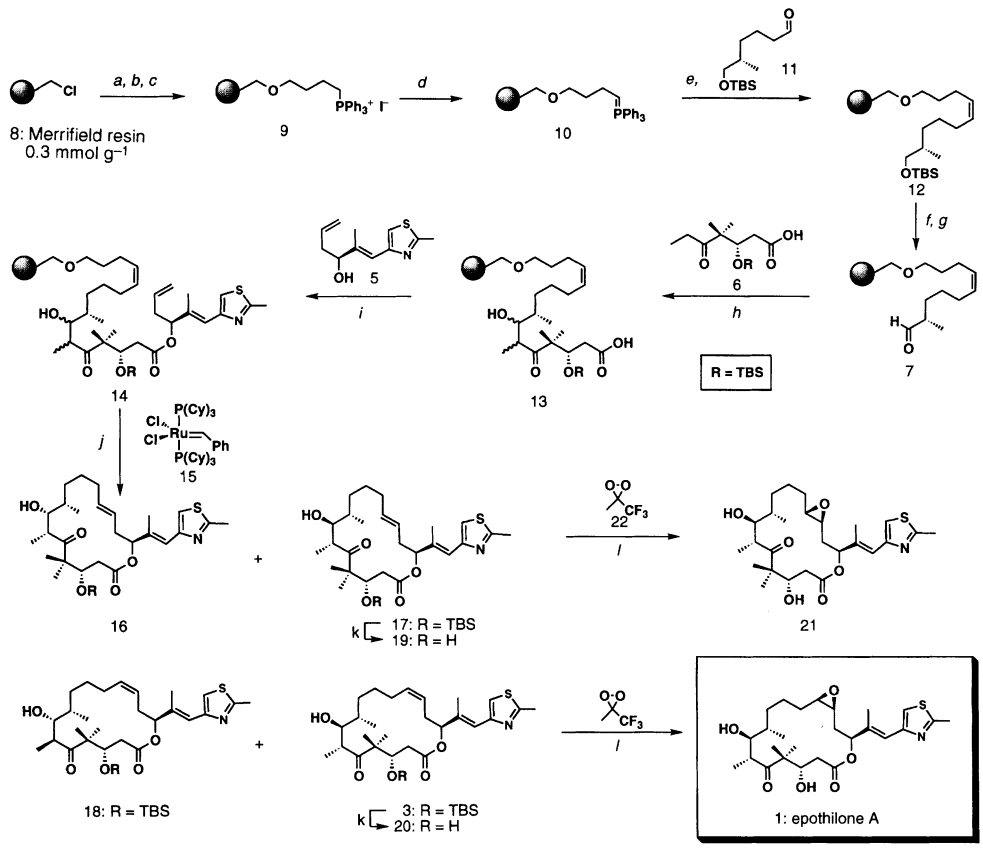

Figure 2 (a) 1,4-butanediol (5.0 equiv.), NaH (5.0 equiv.), *n*-Bu_4NI (0.1 equiv.), DMF, 25 °C, 12 h; (b) Ph_3P (4.0 equiv.), I_2 (4.0 equiv.), imidazole (4.0 equiv.), CH_2Cl_2, 25 °C, 3 h; (c) Ph_3P (10 equiv.), 90 °C, 12 h (>90% for 3 steps based on mass gain of polymer); (d) NaHMDS (3.0 equiv.), THF : DMSO (1 : 1), 25 °C, 12 h; (e) **11** (2.0 equiv.), THF, 0 °C, 3 h (>70% based on aldehyde recovered from ozonolysis); (f) 10% HF·pyridine in THF, 25 °C, 12 h; (g) $(COCl)_2$ (4.0 equiv.), DMSO (8.0 equiv.), Et_3N (12.5 equiv.), −78 → −25 °C (estimated yield ~95% for 2 step; the reaction was monitored by IR analysis of polymer-bound material and by TLC analysis of the products obtained by ozonolysis); (h) **6** (2.0 equiv.), LDA (2.2 equiv.), THF, −78 → −40 °C, 1 h; then add resulting enolate to the resin suspended in a $ZnCl_2$ (2.0 equiv.) solution in THF, −78 → −40 °C, 2 h (~90%; estimated yield, as step g); (i) **5**, (5.0 equiv.), DCC (5.0 equiv.), 4-DMAP (5.0 equiv.), 25 °C, 15 h (80% yield as determined by recovered heterocycle fragments obtained by treatment with NaOMe); (j) **15** (0.75 equiv.), CH_2Cl_2, 25 °C, 48 h (52%; **16** : **17** : **18** : **3** = ~3 : 3 : 1 : 3); (k) 20% TFA in CH_2Cl_2 (v/v), 92% for **19** and 90% for **20**; (l) **22** [methyl(trifluoromethyl)dioxirane, acetonitrile], 0 °C, 2 h (70% for **1**, **45**% for **21**; in addition to these products, the corresponding α-epoxides were also obtained). NaHMDS, sodium bis(trimethylsilyl)amide; DMSO, dimethyl sulphoxide; LDA, lithium diisopropylamide; TBS, *t*-$BuMe_2Si$; 4-DMAP, 4-dimethylaminopyridine; TFA, trifluoroacetic acid. Selected physical data for compound **20**; ^{1}H NMR (400 MHz, $CDCl_3$) δ 6.95 (s, 1 H, ArH), 6.59 (s, 1 H, Ar*CH* = C(CH_3)), 5.44 (ddd, *J* = 10.5, 10.5, 4.5 Hz, 1 H, *CH* = $CHCH_2$), 5.36 (ddd, *J* = 10.5, 10.5, 5.0 Hz. 1 H, *CH* = $CHCH_2$), 5.28 (d, *J* = 9.4 Hz, 1 H, CO_2CH), 4.23 (d, *J* = 11.1 Hz, 1 H, $(CH_3)_2CCl$-H(OH)), 3.72 (m, *CH*OH($CHCH_3$)), 3.43-3.37 (m, 1 H, OH), 3.14 (q, *J* = 6.7 Hz, 1 H, CH_3CH(C = O)), 3.05 (bs, 1 H, OH), 2.72-2.63 (m, 1 H), 2.69 (s, 3 H, CH_3Ar), 2.48 (dd, *J* = 14.8, 11.3 Hz, 1 H, CH_2COO), 2.33 (dd, *J* = 14.8, 2.0 Hz, 1 H, CH_2COO), 2.30-2.13 (m, 2 H) 2.07 (s, 3 H, ArCH = CCH_3), 2.07-1.98 (m, 1 H), 1.80-1.60 (m, 2 H), 1.32 (s, 3 H, $C(CH_3)_2$), 1.36-1.13 (m, 3 H), 1.17 (d, *J* = 6.8 Hz, 3 H, CH_3CH(C = O)), 1.06 (s, 3 H, $C(CH_3)_2$), 0.99 (d, *J* = 7.0 Hz, 3 H, CH_3CHCH_2); ^{13}C NMR (150.9 MHz, $CDCl_3$) δ 220.6, 170.4, 165.0, 151.9, 138.7, 133.4, 125.0, 119.4, 115.8, 78.4, 74.1, 72.3, 53.3, 41.7, 39.2, 38.5, 32.4, 31.7, 27.6, 27.4, 22.7, 19.0, 18.6, 15.9, 15.5, 13.5; infrared (thin film) ν_{max} 3,453, 2,929, 1,733, 1,686, 1,506, 1,464, 1,250, 978 cm^{-1}; $[\alpha]_D^{22}$ − 80.2 (*c* 1.36, $CHCl_3$); HRMS (FAB), calc. for $C_{26}H_{39}CsNO_5S$ (M + Cs^+) 610.1603, found 610.1580.

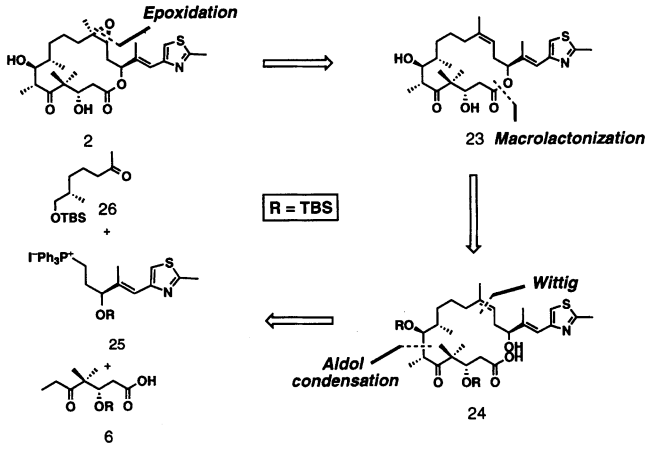

Figure 3 Retrosynthetic analysis of epothilone B (**2**) by a solution-phase strategy. TBS, *t*-BuMe$_2$Si.

(~90% yield, ~1 : 1 ratio). Finally, introduction of the heterocyclic segment **5**[13] onto the growing substrate was achieved by esterification, leading to the required precursor **14** in ~80% yield. Exposure of **14** to $RuCl_2(=CHPh)(PCy_3)_2$, where Cy is cyclohexyl, catalyst (**15**) in CH_2Cl_2 at 25 °C released from the resin olefinic compounds **16–18** and **3** (52% total yield, **16** : **17** : **18** : **3** ≈ 3 : 3 : 1 : 3 as determined by high pressure liquid chromatography (HPLC)). Compounds **16–18** and **3** could be separated either by HPLC or by preparative layer silica gel chromatography, and the two with the correct C6-C7 stereochemistry (that is, **17** and **3**) were desilylated by exposure to TFA (see Fig. 2 legend) to afford epothilone precursors **19** (92%) and **20** (90%), respectively. Epoxidation of **19** and **20** with methyl(trifluoromethyl)dioxirane[27] then furnished epothilone A (**1**, 70%) and its diastereoisomer **21** (45%), respectively. The α-epoxy isomers of **1** and **21** were also obtained in these epoxidation reactions. Pure synthetic epothilone A (**1**) exhibited identical properties (as determined by thin layer chromatography, $[\alpha]_D$ (optical rotation), ^{1}H and ^{13}C NMR, infrared and HRMS (high resolution mass spectrum)) to those of an authentic sample.

The total synthesis of epothilone B (**2**) followed a strategy derived from the retrosynthetic analysis shown in Fig. 3[14]. This strategy called for coupling of intermediates **6**, **25** and **26** via a Wittig olefination, an aldol reaction, and a macrolactonization, followed by epoxidation, and was expected to proceed via intermediates **24** and **23**. This plan was deliberately chosen for its potential to deliver both diastereoisomers at C6-C7 (aldol reaction) and both geometrical isomers at C12-C13 (Wittig reaction) for molecular diversity and biological screening purposes.

The phosphonium salt **25** (K.C.N. *et al.*, unpublished results) was converted to the corresponding ylide by treatment with NaHMDS which reacted with ketone **26** (K.C.N. *et al.*, unpublished results) to afford a mixture of *Z*- and *E*-olefins **27** in 73% yield and ~1 : 1 ratio (by ^{1}H NMR) (Fig. 4). The primary hydroxyl group in **27** was selectively liberated by exposure to CSA (97% yield) and oxidized with SO_3·pyridine–Et_3N–DMSO to afford aldehyde **28** in 95% yield. Treatment of keto acid **6**[13] with excess LDA in THF, followed by reaction with aldehyde **28**, furnished a mixture of four compounds corresponding to the two geometrical isomers of the C12-C13 double bond and the two diastereomeric isomers at C6-C7 in high yield. This mixture was persilylated by exposure to excess TBSOTf and 2,6-lutidine, and then selectively deprotected at the carboxylic acid site (K_2CO_3–MeOH) to afford chromatographically separable (silica gel) carboxylic acids **29** (31% yield from **28**) and its 6*S*,7*R*-diastereoisomer **29a** (30% yield from **28**).

The tris(silylether) **29** was then selectively desilylated at C15 (TBAF, 75% yield) to produce hydroxy acid **24** as a mixture of 12*Z*- and 12*E*-isomers. Macrolactonization[14] of **24** by the Yamaguchi method (2,4,6-trichlorobenzoylchloride, Et_3N, 4-DMAP) resulted in the formation of macrocyclic olefins **30** (40%) and **31** (37%), which were chromatographically separated (silica gel). Exposure of **30** and **31** to TFA led to dihydroxy lactones **32** (89%) and **23** (91%), respectively. Finally, epoxidation of **23** with methyl(trifluoromethyl)dioxirane[27] furnished epothilone B (**2**) together with its α-epoxide epimer **35** in 85% yield and ~5 : 1 ratio in favour of **2**. Pure synthetic epothilone B (**2**) was obtained by preparative layer silica gel chromatography (R_f = 0.24, 4% MeOH in CH_2Cl_2) and exhibited identical properties (thin layer chromatography, $[\alpha]_D$, ^{1}H and ^{13}C NMR, infrared and HRMS) to those of an authentic sample of epothilone B (**2**). Similar treatment of **32** resulted in the formation of epothilones **33** and **34** in 86% yield and ~4 : 1 ratio. The use of *m*CPBA for these epoxidations gave slightly different results leading to **2** and **35** in 66% total yield and ~5 : 1 ratio, and **33** and **34** in 73% total yield and ~4 : 1 ratio.

The synthesized epothilones were tested for their action on tubulin assembly using purified tubulin with an assay[28] developed to amplify differences between compounds more active than taxol. As demonstrated in Fig. 5, both epothilone B (**2**) (EC_{50} = 4.0 ± 1 μM; defined in Fig. 5 legend) and its progenitor **23** (EC_{50} = 3.3 ± 0.2 μM) were significantly more active than taxol (EC_{50} = 15.0 ± 2 μM) and epothilone A (**1**) (EC_{50} =

Table 1 Relative activities of epothilones A (1) and B (2) as compared with synthetic analogues 23, 20, 32, 34 and taxol

Compound	Induction of tubulin assembly*	Inhibition of human ovarian carcinoma cell growth†			
		Parental	Taxol-resistant		
			β-tubulin mutants		MDR-line
		1A9	1A9PTX10	1A9PTX22	A2780AD
	EC_{50} (μM) + s.d.		IC_{50} nM (relative resistance)		
1	14 ± 0.4	2.0	19 (9.5)	4.2 (2.1)	2.4 (1.2)
2	4.0 ± 0.1	0.040	0.035 (0.88)	0.045 (1.1)	0.040 (1.0)
23	3.3 ± 0.2	2.0	33 (17)	3.5 (1.8)	1.5 (0.80)
20	25 ± 1	25	>100 (>4)	75 (3.0)	22 (0.88)
32	39 ± 2	48	>100 (>2)	75 (1.6)	24 (0.50)
34	22 ± 0.9	3.5	30 (8.6)	5.5 (1.6)	3.0 (0.86)
Taxol	15 ± 2	2.0	50 (25)	43 (22)	> 100 (>50)

* See Fig. 5.

† The growth of all cell lines was evaluated by quantitation of the protein in microtitre plates[4]. The parental cell line 1A9, a clone of the A2780 cell line, was used to select two taxol resistant sublines (1A9PTX10 and 1A9PTX22)[29]. These sublines were selected by growth in the presence of taxol and verapamil, a P-glycoprotein modulator. Two distinct point mutations in the β-tubulin isotype M40 gene were identified. In 1A9PTX10 amino acid residue 270 was changed from Phe (TTT) to Val (GTT), and in 1A9PTX22 residue 364 was changed from Ala (GCA) to Thr (ACA). The A2780AD line is a multi-drug resistant (MDR) line expressing high levels of P-glycoprotein[30]. Relative resistance refers to the ratio of the IC_{50} value obtained with a resistant cell line to that obtained with the parental cell line.

14.0 ± 0.4 μM), whereas compounds **34**, **20** and **32** were less effective than taxol.

Preliminary cytotoxicity experiments with 1A9, 1A9PTX10 (β-tubulin mutant)[29], 1A9PTX22 (β-tubulin mutant)[29] and A2780AD cell lines revealed a number of interesting results (Table 1). Despite its high potency in the tubulin assembly assay, compound **23** did not display the potent cytotoxicity of **2** against 1A9 cells, being similar to **1** and taxol. These data suggest that whereas the C12-C13 epoxide is not required for the epothilone–tubulin interaction, it may play an important role in localizing the agent to its target within the cell. Like the naturally occurring epothilones **1** and **2**, analogue **23** showed significant activity against the MDR line A2780AD and the altered β-tubulin-expressing cell lines 1A9PTX10 and 1A9PTX22, suggesting, perhaps, different contact points for the epothilones and taxol with tubulin (that is, stronger binding of epothilones around residue 364 than around 270 relative to taxoids).

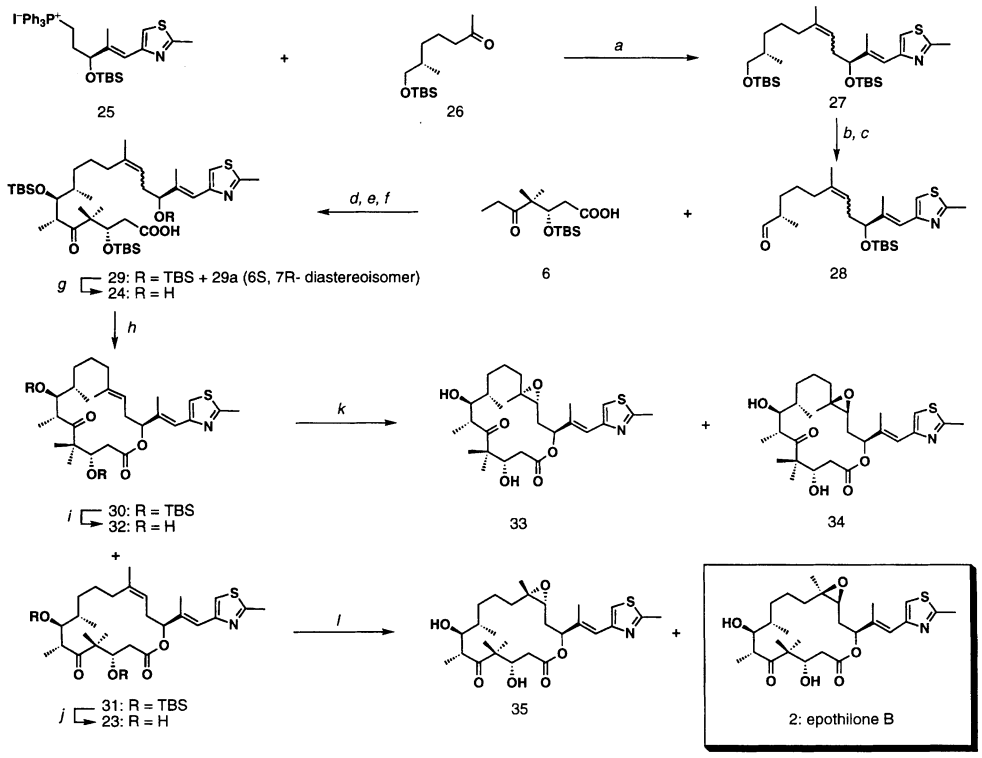

Figure 4 (a) **25** (1.5 equiv.), NaHMDS (1.5 equiv.), THF, 0 °C, 15 min; then add **26** (1.0 equiv.), −20 °C, 12 h, 73% (*Z* : *E* ~1 : 1); (b) CSA (1.0 equiv.), CH_2Cl_2 : MeOH (1 : 1), 0 °C, 1 h; then 25 °C, 0.5 h, 97%; (c) SO_3·pyr. (2.0 equiv.), DMSO (10 equiv.), Et_3N (5 equiv.), CH_2Cl_2, 25 °C, 0.5 h, 95%; (d) LDA (3.0 equiv.), THF, 0 °C, 15 min; then **6** (1.2 equiv. in THF), −78 → −40 °C, 0.5 h; then **28** (1.0 equiv. in THF), −78 °C; (e) TBSOTf (3.0 equiv.), 2,6-lutidine (5.0 equiv.), CH_2Cl_2, 0 °C, 2 h; (f) K_2CO_3 (2.0 equiv.), MeOH, 25 °C, 15 min, 31% of **29** from **28** and 30% of **29a** from **28**; (g) TBAF (6.0 equiv.), THF, 25 °C, 8 h, 75%; (h) 2,4,6-trichlorobenzoylchloride (2.0 equiv.), Et_3N (2.0 equiv.), THF, 0 °C, 1 h; then add to a solution of 4-DMAP (10.0 equiv. in toluene, 0.002 M), 25 °C, 12 h, 40% of **30** and 37% of **31**; (i) 20% TFA (by volume) in CH_2Cl_2, −10 → −0 °C, 1 h, 89%; (j) same as *i*, 91%; (k) methyl(trifluoromethyl) dioxirane, acetonitrile, 0 °C, 86% (**33** : **34** ~1 : 1 diastereoisomers) or *m*CPBA (1.5 equiv.), benzene. 3 °C, 2 h, 73% (**33** : **34** ~4 : 1 ratio of stereoisomers); (l) methyl(trifluoromethyl)dioxirane, acetonitrile, 0 °C, 85% (**2** : **35** ~5 : 1 ratio of diastereoisomers) or *m*CPBA (1.5 equiv.), benzene, 3 °C, 2 h, 66% (**2** : **35** ~5 : 1 ratio of diastereoisomers); NaHMDS, sodium bis(trimethylsilyl)amide; CSA, camphorsulphonic acid; DMSO, dimethyl sulphoxide; LDA, lithium diisopropylamide; TBS,*t*-$BuMe_2Si$; TBSOTf, *t*-$BuMe_2SiOSO_2CF_3$; TBAF, tetra-*n*-butylammonium fluoride; 4-DMAP, 4-dimethylaminopyridine; *m*CPBA, 3-chloroperoxybenzoic acid; TFA, trifluoroacetic acid. Selected physical data for compound **23**: ^{1}H NMR (600 MHz, $CDCl_3$) δ 6.94 (s, 1 H, SCH = C), 6.57 (s, 1 H, C*H* = CCH_3), 5.20 (d, *J* = 9.7 Hz, 1 H, CH_2COOCH), 5.13 (dd, *J* = 9.6, 4.6 Hz, 1 H, CH_3C = $CHCH_2$), 4.28 (d, *J* = 9.7 Hz, 1 H, $(CH_3)_2CCHOH$), 3.71 (s, 1 H, *CH*OH), 3.47 (bs, 1 H, OH), 3.15 (q, *J* = 6.8 Hz, 1 H, $C(O)CHCH_3$), 3.04 (bs, 1 H, OH), 2.68 (s, 3 H, N = $C(CH_3)S$), 2.62 (ddd, *J* = 15.0, 10.2, 10.1 Hz, 1 H, CH_2CH = CCH_3), 2.45 (dd, *J* = 14.7, 11.1 Hz, 1 H, CH_2COOCH), 2.38–2.24 (m, 1 H), 2.28 (dd, *J* = 14.8, 2.2 Hz, CH_2COOCH), 2.22 (d, *J* = 14.9 Hz, 1 H, $CH_2C(CH_3)$ = $CHCH_2$), 2.06 (s, 3 H, CH = CCH_3), 1.90–1.84 (m, 1 H), 1.76–1.69 (m, 1 H), 1.65 (s, 3 H, $CH_2C(CH_3)$ = CH), 1.33 (s, 3 H, $C(CH_3)_2$), 1.32–1.22 (m, 4 H), 1.19 (d, *J* = 6.8 Hz, 3 H, $CH(CH_3)$), 1.06 (s, 3 H, $C(CH_3)_2$), 1.00 (d, *J* = 7.0 Hz, 3 H, $CH(CH_3)$); ^{13}C NMR (150.9 MHz, $CDCl_3$) δ 220.4, 170.2, 164.9, 151.8, 139.1, 138.3, 120.8, 119.1, 115.5, 78.9, 74.1, 72.3, 53.6, 41.7, 39.7, 32.6, 31.8, 31.7, 25.4, 23.0, 19.1, 18.1, 16.0, 15.8, 13.5; infrared (thin film) ν_{max} 3,460, 2,954, 2,919, 1,725, 1,684, 1,455, 1,379, 1,290, 1,249, 1,184, 1,143, 1,043, 1,008, 973, 750 cm^{-1}; $[\alpha]_D^{22}$ − 91.5 s, (c 0.3, $CHCl_3$); HRMS (FAB) *m/e* 492.2795, (M + H$^+$) calc. for $C_{27}H_{41}NO_5S$ 492.2784.

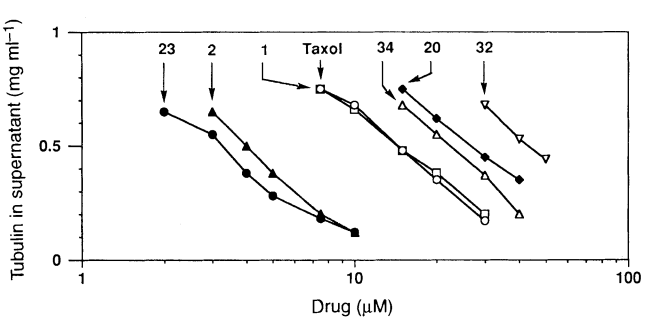

Figure 5 The tubulin assembly assay was performed essentially as described previously[28]. Reaction mixtures contained purified tubulin at 1.0 mg ml^{-1}, 0.4 M monosodium glutamate, 5% dimethyl sulphoxide, and varying drug concentrations. Each compound was evaluated in three different experiments and average values are shown. The EC_{50} is defined as the drug concentration that causes 50% of the tubulin to assemble into polymer. In the absence of drug, <5% of the tubulin was removed by centrifugation, while with high concentrations of the most active drugs, >95% of the protein formed polymer. This suggests that at least 90% of the tubulin had the potential to interact with epothilones and taxoids. Although the EC_{50} value obtained for taxol was higher than that obtained in an alternate assay[3], the agent's role in these experiments was only as a control. The numbers on the curves correspond to compound numbers in the text.

The solid-phase synthesis of epothilone A (**1**) described here represents a new concept for the total synthesis of natural products, traces a highly efficient pathway to the naturally occurring epothilones, and opens the way for the generation of large combinatorial epothilone libraries. The biological results demonstrate that more potent microtubule binding analogues than the parent epothilones can be obtained (for example, compound **23**) by chemical synthesis. Furthermore, our findings point to lipophilic substituents rather than the epoxide moiety as important elements for binding activity. The role of the epoxide in the cytotoxicity of epothilones, however, still remains to be elucidated. □

Received 3 April; accepted 17 April 1997.

1. Höfle, G. *et al.* Epothilone A and B—novel 16-membered macrolides with cytotoxic activity: isolation, crystal structure, and conformation in solution. *Angew. Chem. Int. Edn. Engl.* **35,** 1567–1569 (1996).
2. Grever, M. R., Schepartz, S. A. & Chabner, B. A. The national cancer institute: cancer drug discovery and development program. *Semin. Oncol.* **19,** 622–638 (1992).
3. Bollag, D. M. *et al.* Epothilones, a new class of microtubule-stabilizing agents with a Taxol-like mechanism of action. *Cancer Res.* **55,** 2325–2333 (1995).
4. Kowalski, R. J., Giannakakou, P. & Hamel, E. Activities of the microtubule-stabilizing agents epothilones A and B with purified tubulin and in cells resistant to paclitaxel (Taxol). *J. Biol. Chem.* **272,** 2534–2541 (1997).
5. Nicolaou, K. C., He, Y., Vourloumis, D., Vallberg, H. & Yang, Z. An approach to epothilones based on olefin metathesis. *Angew. Chem. Int. Edn. Engl.* **35,** 2399–2401 (1996).
6. Meng, D., Sorensen, E. J., Bertinato, P. & Danishefsky, S. J. Studies toward a synthesis of epothilone A: use of hydropyran templates for the management of acyclic stereochemical relationships. *J. Org. Chem.* **61,** 7998–7999 (1996).
7. Bertinato, P., Sorensen, E. J., Meng, D. & Danishefsky, S. J. Studies toward a synthesis of epothilone A: stereocontrolled assembly of the acyl region and models for macrocyclization. *J. Org. Chem.* **61,** 8000–8001 (1996).
8. Schinzer, D., Limberg, A. & Böhm, O. M. Studies toward the total synthesis of epothilones: asymmetric synthesis of the key fragments. *Chem. Eur. J.* **2,** 1477–1482 (1996).
9. Mulzer, J. & Mantoulidis, A. Synthesis of the C(1)-C(9) segment of the cytotoxic macrolides epothilon A and B. *Tetrahedr. Lett.* **37,** 9179–9182 (1996).
10. Claus, E., Pahl, A., Jones, P. G., Meyer, H. M. & Kalesse, M. Synthesis of the C1-C9 segment of epothilons. *Tetrahedr. Lett.* **38,** 1359–1362 (1997).
11. Gabriel, T. & Wessjohann, L. The Chromium-Reformatsky reaction: asymmetric synthesis of the aldol fragment of the cytotoxic epothilons from 3-(2-bromoacyl)-2-oxazolidinones. *Tetrahedr. Lett.* **38,** 1363–1366 (1997).
12. Balog, A. *et al.* Total synthesis of (-)-epothilone A. *Angew. Chem. Int. Edn Engl.* **35,** 2801–2803 (1996).
13. Yang, Z., He, Y., Vourloumis, D., Vallberg, H. & Nicolaou, K. C. Total synthesis of epothilone A: the olefin metathesis approach. *Angew. Chem. Int. Edn. Engl.* **36,** 166–168 (1997).
14. Nicolaou, K. C., Sarabia, F., Ninkovic, S. & Yang, Z. Total synthesis of epothilone A: the macrolactonization approach. *Angew. Chem. Int. Edn. Engl.* **36,** 525–527 (1997).
15. Schinzer, D., Limberg, A., Bauer, A., Böhm, O. M. & Cordes, M. Total synthesis of (−)-epothilone A. *Angew. Chem. Int. Edn Engl.* **36,** 523–524 (1997).
16. Meng, D. *et al.* Remote effects in macrolide formation through ring-forming olefin metathesis: an application to the synthesis of fully active epothilone congeners. *J. Am. Chem. Soc.* **119,** 2733–2734 (1997).
17. Horwitz, S. B., Fant, J. & Schiff, P. B. Promotion of microtubule assembly *in vitro* by taxol. *Nature* **277,** 665–667 (1979).
18. Nicolaou, K. C., Dai, W.-M. & Guy, R. K. The chemistry and biology of Taxol. *Angew. Chem. Int. Edn. Engl.* **33,** 15–44 (1994).
19. Su, D.-S. *et al.* Total synthesis of (−)-epothilone B: an extension of the Suzuki coupling method and insights into structure-activity relationships of the epothilones. *Angew. Chem. Int. Edn. Engl.* **36,** 757–759 (1997).
20. Grubbs, R. H., Miller, S. J. & Fu, G. C. Ring-closing metathesis and related processes in organic synthesis. *Acc. Chem. Res.* **28,** 446–452 (1995).
21. Miller, S. J., Blackwell, H. E. & Grubbs, R. H. Application of ring-closing metathesis to the synthesis of rigidified amino acids and peptides. *J. Am. Chem. Soc.* **118,** 9606–9614 (1996).
22. Xu, Z., Johannes, C. W., Salman, S. S. & Hoveyda, A. H. Enantioselective total synthesis of antifungal agent Sch 38516. *J. Am. Chem. Soc.* **118,** 10926–10927 (1996).
23. van Maarseveen, J. H. *et al.* Solid phase ring-closing metathesis: cyclization/cleavage approach towards a seven membered cycloolefin. *Tetrahedr. Lett.* **37,** 8249–8252 (1996).
24. Miller, J. F., Termin, A. & Piscopio, A. D. Ester enolate Claisen-ring closing metathesis route to functionalized carbocycles and heterocycles. Presented at 213th Am. Chem. Soc. Natl Meeting, San Francisco. 13–17 April (1997).
25. Schuster, M., Pemerstorfer, J. & Blechert, S. Ruthenium-catalyzed metathesis of polymer-bound olefins. *Angew. Chem. Int. Edn. Engl.* **35,** 1979–1980 (1996).
26. Bernard, M. & Ford, W. T. Wittig reagents bound to cross-linked polystyrenes. *J. Org. Chem.* **48,** 326–332 (1983).
27. Yang, D., Wong, M.-K. & Yip, Y.-C. Epoxidation of olefins using methyl(trifluoromethyl)dioxirane generated *in situ*. *J. Org. Chem.* **60,** 3887–3889 (1995).
28. Lin, C. M. *et al.* A convenient tubulin-based quantitative assay for paclitaxel (Taxol) derivatives more effective in inducing assembly than the parent compound. *Cancer Chemother. Pharmacol.* **38,** 136–140 (1996).
29. Giannakakou, P. *et al.* Paclitaxel resistant human ovarian cancer cells have mutant β-tubulins that exhibit impaired paclitaxel driven polymeriazation. *J. Biol. Chem.* (in the press).
30. Rogan, A. M. *et al.* Reversal of adriamycin resistance by verapamil in human ovarian cancer. *Science* **244,** 994–996 (1984).

Acknowledgements. We thank G. Höfle and Merck Research Laboratories for gifts of epothilones A and B; and D. H. Huang and G. Siuzdak for NMR and mass spectroscopic assistance, respectively. This work was supported by the NIH, The Skaggs Institute for Chemical Biology and the CaP CURE Foundation, and fellowships from the Ministerio de Educación y Ciencia (Spain) (J.P.), Fundación Ramón Areces (Spain) (F.S.) and Novartis (D.V.), and grants from Merck, DuPont-Merck, Schering Plough, Hoffmann La Roche and Amgen.

Correspondence and requests for materials should be addressed to K.C.N. at Scripps Research Institute.

Evolution of the nitrogen cycle and its influence on the biological sequestration of CO_2 in the ocean

Paul G. Falkowski

Oceanographic and Atmospheric Sciences Division, Brookhaven National Laboratory, Upton, New York 11973, USA

Over geological time, photosynthetic carbon fixation in the oceans has exceeded respiratory oxidation of organic carbon. The imbalance between the two processes has resulted in the simultaneous accumulation of oxygen in, and drawdown of carbon dioxide from, the Earth's atmosphere, and the burial of organic carbon in marine sediments[1–3]. It is generally assumed that these processes are limited by the availability of phosphorus[4,5], which is supplied by continental weathering and fluvial discharge[5–7]. Over the past two million years, decreases in atmospheric carbon dioxide concentrations during glacial periods correlate with increases in the export of organic carbon from surface waters to the marine sediments[8–11], but variations in phosphorus fluxes appear to have been too small to account for these changes[12,13]. Consequently, it has been assumed that total oceanic primary productivity remained relatively constant during glacial-to-interglacial transitions, although the fraction of this productivity exported to the sediments somehow increased during glacial periods[12,14]. Here I present an analysis of the evolution of biogeochemical cycles which suggests that fixed nitrogen, not phosphorus, limits primary productivity on geological timescales. Small variations in the ratio of nitrogen fixation to denitrification can significantly change atmospheric carbon dioxide concentrations on glacial-to-interglacial timescales. The ratio of these two processes appears to be determined by the oxidation state of the ocean and the supply of trace elements, especially iron.

Globally, nitrogen and phosphorus are the two elements that potentially limit the biologically mediated carbon assimilation in the oceans by photoautotrophs. It is frequently argued that, as N_2 is abundant in both the ocean and atmosphere, and, in principle, can be biologically reduced to the equivalent of NH_3 by N_2-fixing cyanobacteria (that is, diazotrophs), nitrogen cannot be limiting on geological timescales[4,15,16]. It then follows that phosphorus, which has no significant atmospheric source, must ultimately limit biological productivity. The underlying assumptions of these tenets should, however, be considered within the context of the evolution of biogeochemical cycles and the manifestations of those cycles in the contemporary ocean.

Virtually all fixed inorganic nitrogen in the contemporary ocean is oxidized to nitrate. Where did the nitrate come from? Although, in the Archaean atmosphere, electrical discharge or bolide impacts might have promoted NO formation from reaction between N_2 and CO_2, the yield for the reaction is low[17]. NH_3 in the Archaean atmosphere would have photodissociated, driven by ultraviolet radiation[17]; however, N_2 would have been stable and abundant[17,18]. N_2 can be biologically reduced to NH_3 via the enzyme nitrogenase. Biological N_2 fixation is a strictly anaerobic process[19], and the sequence of the genes encoding the catalytic subunits for nitrogenase is highly conserved in cyanobacteria and other eubacteria, strongly suggesting an ancient, common ancestral origin[20]. The antiquity and homology of nitrogen fixation capacity also implies that fixed inorganic nitrogen in the Archaean and early Protozeroic oceans was scarce before the evolution of diazotrophic organisms; that is, there was strong evolutionary selection for N_2 fixation.